Journal of Power Sources 195 (2010) 6349–6355

Contents lists available at ScienceDirect

Journal of Power Sources

journal homepage: www.elsevier.com/locate/jpowsour

Impact of synchrotron radiation on fuel cell operation in imaging experiments

Armin Schneider[a,*], Christian Wieser[a], Jörg Roth[a], Lukas Helfen[b]

[a] Adam Opel GmbH, GM Alternative Propulsion Center Europe, 65423 Rüsselsheim, Germany
[b] Institute for Synchrotron Radiation - ANKA, Karlsruhe Institute of Technology, 76021 Karlsruhe, Germany

ARTICLE INFO

Article history:
Received 11 January 2010
Received in revised form 31 March 2010
Accepted 11 April 2010
Available online 18 April 2010

Keywords:
Synchrotron imaging
Fuel cell
Water management
Diagnostics
Degradation

ABSTRACT

For the clarification of water transport mechanisms in operating fuel cells, synchrotron radiation computed tomography (SR-CT) was applied. A novel fuel cell has been designed that exposes the entire active area (7 mm^2) to the SR beam while at the same time allowing for full fuel cell operation during the imaging experiment. This micro fuel cell has been qualified successfully prior to the SR imaging experiments. The cell voltage was 600 mV at 0.2 A cm^{-2} (open circuit voltage, OCV > 950 mV) and the operation was stable for hours. However, under SR beam exposition for in situ imaging, severe cell performance degradation within minutes has been reproducibly observed. Even after the SR beam had been switched-off cell operation remained irreversibly degraded whilst OCV could be recovered. Preliminary results indicate a higher degradation sensitivity of the cathode side of the cell. Apparently, the unique setup of the experiment which exposes an operating fuel cell with the entire active area to the SR beam reveals otherwise unnoticeable degradation mechanisms. It may have to be concluded that the very same materials degrade heavily during beam exposure that are subject of the imaging investigation. Consequently, the applicability of SR imaging to study water transport in porous fuel cell materials has to be revisited critically. This publication describes the observations made during fuel cell operation under SR beam exposure and discuss potential mechanisms that may cause beam-induced performance degradation.

1. Introduction

Water visualization in operating fuel cells was identified as being important for understanding the fundamental transport mechanisms within the different components of a polymer electrolyte fuel cell. Various experimental techniques to determine and/or monitor the water distribution in operating fuel cells have been developed and published. These methods comprise imaging methods, for instance neutron and synchrotron radiography, nuclear magnetic resonance tomography as well as several optical methods, and non-imaging analytical methods, e.g. Raman and IR spectroscopy, X-ray diffraction and electrical resistivity measurements. Comprehensive overviews with continuative references have been published by St-Pierre [1] and Bazylak [2]. From the imaging methods neutron radiography is widely used. Fuel cell hardware of any active area dimensions can be investigated with small, if any, influence on fuel cell performance and fuel cell behavior. The only disadvantage is the spatial resolution which is currently limited to approximately 25 μm. This resolution is not sufficient to visualize water within the pore structure of typical gas diffusion media with average pore diameters between 10 and 30 μm and fiber diameters that typically range between 5 and 10 μm. In order to capture the dynamics of liquid water transport and liquid/solid interaction in that scale, the resolution has to be in the order of half of the fiber diameter or higher. Synchrotron radiography, for instance, offers high spatial resolutions down to 0.5 μm [3]. These resolutions are also appropriate for resolving a layer thickness as small as 100–200 μm for typical fuel cell diffusion media. Besides spatial resolution, understanding transport phenomena in the anisotropic diffusion media requires 3D imaging instead of the more typical 2D investigations at sufficient temporal resolution to cover the dynamic processes. Synchrotron micro-tomography seems to be a good candidate to provide these capabilities.

Several investigations regarding water visualization in operating fuel cells by synchrotron radiography have been published. Manke et al. investigated the 2D water evolution and transport in an operating fuel cell of technical size [4]. They used a fuel cell with 100 cm^2 active area but visualized an area of about 7 mm × 7 mm through an 8 mm hole in the metallic end plates. The beam exposure was 1 s for each 2D image having a pixel size down to 1.5 μm. They found a periodic water droplet transport behavior. Furthermore, Hartnig et al. published 2D images of the water evolution and transport in a 7 mm × 7 mm cross-section of an operating cell of 12 cm^2 active area [5,6], again with a pixel size down to 1.5 μm. As result they show a 2D liquid water formation resolved by different

* Corresponding author. Tel.: +49 6142 7538 24; fax: +49 6142 7543 59.
E-mail address: armin.schneider@opel.de.com (A. Schneider).

0378-7753/$ – see front matter © 2010 Elsevier B.V. All rights reserved.
doi:10.1016/j.jpowsour.2010.04.032

layers of the fuel cell. Mukaide et al. [7] investigated an operating fuel cell with different diffusion layers and found different water distributions. The active area of the fuel cell was 20 mm × 7.5 mm, but the imaged area was just a fraction of that (approx. one-eighth of the active area). The exposition time for each image was 1 s and the pixel resolution approx. 6 μm. 2D images were taken from two directions in-plane and through-plane. In contrast to the above publications, Flückiger et al. [3] determined a 3D liquid water distribution in hydrophobic and hydrophilic diffusion layers with a pixel resolution of 1 μm. Therefore, they constructed a simplified circular fuel cell with an active area of 7 mm^2. In order to generate water the cell has been short-circuited, i.e. apparently current and voltage have not been controlled or measured actively. Due to the minimized cell it is the first published operating fuel cell setup where the entire active area was exposed to synchrotron radiation (SR).

The state-of-the-art as described above may not consider all cell related and imaging needs comprehensively. Either technically relevant cells with designs used in actual applications are operated during the imaging but only 2D data sets of a fraction of the total active area are provided. Alternatively, a whole miniaturized cell is imaged, but it does not exhibit technically relevant cell designs and is not operated under controlled fuel cell operation during the imaging process.

Hence, the intention of the work presented here was to design a fuel cell for 3D imaging of the full active area and still have sufficient spatial and temporal resolution to visualize the dynamic water evolution and transport. Furthermore, the design of the miniaturized cell reflects the actual design of technical fuel cells like a sealed parallel channel flow field with application relevant channel and land geometries and adjustable cell compression. To image under relevant operating conditions, the peripheral setup allows for measuring and controlling voltage or current as well as temperature, pressure and gas flow.

2. Experimental

SR imaging has been performed at the European Synchrotron Radiation Facility in Grenoble, France, utilizing beam line ID19 which is specifically equipped for micro-tomography [8] and also fibrous materials have already been investigated successfully [9]. A full 3D tomographic image of an object is obtained by turning the object during beam exposure and making a series of 2D projection images for each individual object/beam angle by means of a charge-coupled device (CCD) optically coupled to a scintillator crystal. The 3D information can be reconstructed from this series of 2D images. In the case of the fuel cell the design of the cell and the peripheral equipment have to comply with the need to rotate the objects during the imaging process. Despite of possible spatial resolutions down to 0.5 μm [10] a trade-off between spatial and temporal resolution has been made to meet the requirement that dynamic transport processes have to be captured. Based on the steady-state requirement for fuel cell operation, it has been estimated that a full tomography needs to be completed after less than one minute (see e.g. [4]). Hence, a pixel size of 2.8 μm has been chosen with a CCD operation in binning mode (summing 4 pixels of each 1.4 μm effective size) which reduces exposure time per image and, hence, enables getting down to approx. 30 s for a full set of 2D projection images. Another 30 s were needed for the acquisition of correction images of the beam profile and CCD dark images. Therefore, the data needed to reconstruct a full 3D tomography could be obtained every 60 s which is expected to provide sufficient temporal resolution to visualize transient water transport phenomena. The beam has a rectangular cross-section of approx. 1.5 mm in height and 3 mm in width. The beam energy was adjusted to 20.5 keV and the sample distance to the detector was 20 mm to provide edge enhancement due to phase contrast [8]. For 3D image reconstruction, a standard filtered backprojection algorithm was applied ("pyHST" provided by ESRF [11]).

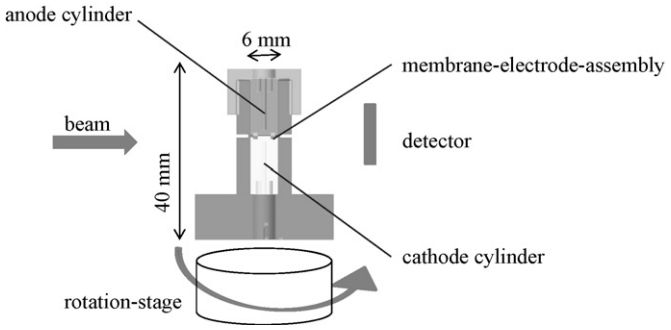

Fig. 1. SR imaging principle with cross-sectional view of the micro fuel cell.

To combine the requirements of 3D SR imaging and fuel cell operation, a miniaturized fuel cell with a circular shape and an active area of approximately 0.07 cm^2 was designed (Fig. 1). The active area diameter was restricted to 3 mm due to the beam geometry mentioned above. To provide controlled and adjustable cell compression, the cell housing was equipped with an adjustable screw cap. For minimizing beam attenuation polypropylene and small material thickness at the exposed locations have been used.

The flow fields of both anode and cathode are manufactured from carbon composite material and have the shape of cylinders with an outer diameter of 6 mm to make them fit into the cell housing. Machined into one end is the flow field and inside the other end are the connections for the gas inlet and outlet, current collector, thermocouple and heater elements. The flow field has two straight parallel gas channels with a length of 3 mm and a depth and width of 0.5 mm separated by a 0.5 mm land. The gas inlet and outlet boreholes have 0.5 mm diameter. The cell is sealed gas-tight around the perimeter of the active area by flat Viton rings inserted into a lining groove. The used polymer electrolyte membrane was a perfluorosulfonic acid (PFSA) type membrane with a thickness of 25 μm. As a gas diffusion electrode a catalyst coated diffusion medium (CCDM) has been used comprised of a carbon paper with a microporous layer and a catalyst layer with an overall thickness of 240 μm. The platinum loading was 0.4 mg cm^{-2} for both anode and cathode side. The components of the cell hardware and the softgoods are illustrated in Fig. 2.

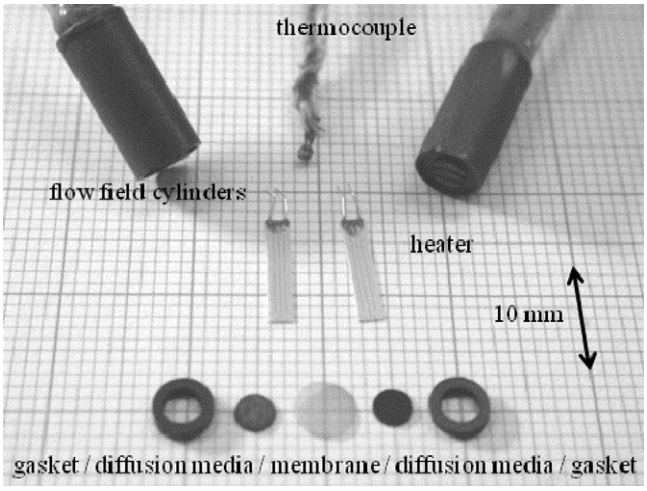

Fig. 2. The components of the micro fuel cell.

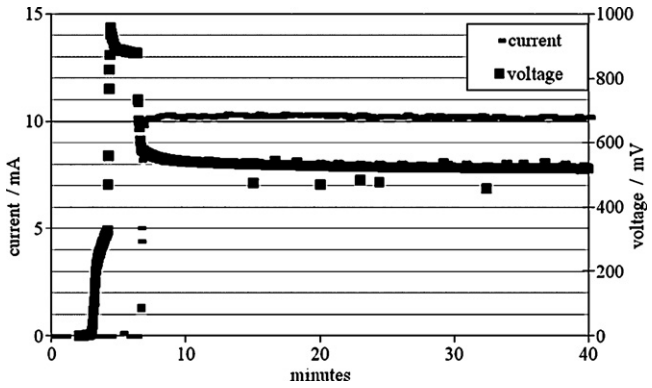

Fig. 3. Representative startup procedure of the micro fuel cell. A constant current of 10 mA was adjusted which is equivalent to a current density of 0.14 mA cm^{-2}.

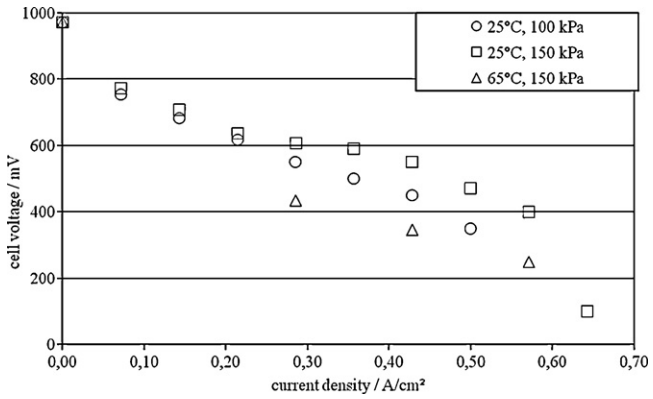

Fig. 4. Polarization curves at different operating conditions. In all cases no gas humidification was provided and the gas stoichiometry was 2.

Peripheral equipment and data acquisition have been realized such that full fuel cell operation from the remote control room at the beamline was possible. In order to ensure stable galvanostatic operation of the tiny fuel cell a suitable electronic load which covers the automotive relevant range of current densities up to 1.5 A cm^{-2} in the 0–1 V voltage range and a control accuracy of ±7 mA cm^{-2} has been developed. Both anode and cathode have been equipped with heater elements and thermocouples for temperature control. Gas mass flow controllers (MFC) where used to control the flow rates and stoichiometries, respectively. The lowest adjustable flow rates with the used MFC allowed for anode stoichiometries as little as 2 at a current density of 0.14 A cm^{-2}. Highest flow rates allowed a cathode stoichiometry of 5 at 1.5 A cm^{-2}. Pressure controllers were installed at the cell outlets and two additional pressure sensors at the gas inlets. The sealing system of the cell allowed pressurized operation up to 200 kPa$_{abs}$. In order to simplify the peripheral equipment with regard to the limitations at the beamline and to avoid imaging artifacts caused by externally introduced condensation water, reactant humidification was not implemented, and the cell has been operated with dry inlet gases.

3. Results

3.1. Cell performance without SR

In order to justify that findings from the imaging with the micro fuel cell can be transferred to technical fuel cell applications, the miniaturized cell was required to work properly in terms of exhibiting typical open circuit voltages (OCV) > 950 mV and reasonable polarization curves. Hence, the cell has been qualified in the fuel cell laboratory before being transferred to the SR facility. Fig. 3 exemplarily shows a representative startup procedure and corresponding micro fuel cell response. The cell has been operated at room temperature and ambient pressure. After starting reactant flow the OCV jumps to 955 mV and stabilizes in less than a minute at approx. 880 mV, which is typically observed with new membrane electrode assemblies (MEA) prior to the startup procedure. Afterwards, the cell load was set to a constant current density of 0.14 A cm^{-2} resulting in a stable voltage of 520 mV after a few minutes. The gas stoichiometry for both air and hydrogen at the given load was at approx. 5 so that the operating conditions were very dry. In the course of fuel cell operation the load was switched off regularly to measure the OCV in order to ensure that no crossover leak or short-circuit (e.g. by membrane puncturing) has occurred. As a criterion for an intact cell after the startup procedure a minimum OCV of 900 mV has been defined.

Further qualification of the cell required execution of polarization curves and variation of operating conditions. Fig. 4 shows representative polarization curves under varying conditions. The stoichiometry during all curves was 2 for anode and cathode side. All polarization curves in Fig. 4 have been executed with the same cell build, i.e. without disassembly of the cell, and before each acquisition of a polarization curve it has been ensured that the open circuit voltage was above 960 mV. Independent of the operating conditions, all polarization curves shows similar performance below 0.2 A cm^{-2}. As a baseline, ambient conditions have been applied. Increasing pressure to 150 kPa improves performance visibly. Furthermore, by setting the temperature to 65 °C at elevated pressure a significantly reduced performance was observed. Besides the losses in the kinetic region which may indicate a suboptimal interface between the CCDM and the membrane in the assembly for the micro fuel cell, it has to be assumed that the operation with unhumidified gases is a one major source of performance limitation.

The reproducibility of the fuel cell assemblies was demonstrated with three different identical cell builds where the spread between each built is sufficiently small as the maximum voltage difference to the average value for a specific load case is 26 mV. Based on the results from the qualification experiments it has been decided that the cell should be usable for the purpose of imaging water in an operating fuel cell where liquid water in the fibrous diffusion medium (DM) has been generated electrochemically and occurrence and transport of water in the porous media is relevant for the application.

3.2. Cell performance under SR exposure

Cell and peripheral equipment were transferred to the ID 19 micro-tomography beamline at the ESRF where proper teststand and cell operation have been checked and lab performance has been reproduced. Each individual imaging experiment has been executed with fresh, unused softgoods, and prior to beam exposition the cell was operated at constant current conditions at room temperature and ambient pressure until stable conditions were reached. However, as soon as the cell was exposed to the SR beam cell performance decayed instantly and severely which could be observed reproducibly. Due to the high rate of this decay, a systematic study of the degradation observation by exposing the fuel cell components individually to the beam, was done prior to any further imaging experiment, as described in the following.

A slit aperture has been used to expose just fractions of the fuel cell to the beam in order to irradiate the individual softgood layers instead of the entire fuel cell and thereby identify the component which reacts sensitive to beam exposure. For this purpose, the slit aperture of the beamline has been closed in such a way that the effective cross-section of the beam was reduced to a height of

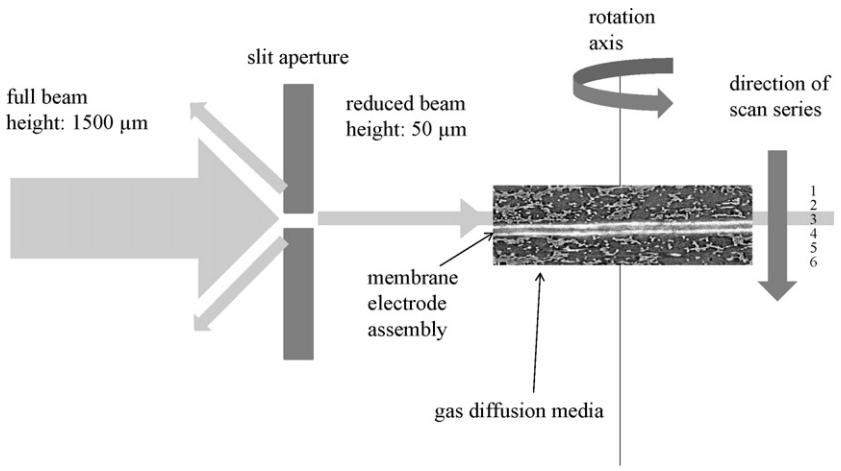

Fig. 5. Schematic illustration of a scan series. The example shows the beam position during the 3 scan.

50 µm. By moving the beam from the top to the bottom of the cell in succeeding scans the sensitivity of the cathode side vs. the anode side of the cell to the beam exposition could be separated. Since the thickness of the compressed softgood assembly, comprising the MEA and the anode and cathode DM, was 350 µm (30% compression) and the height of the beam was set to 50 µm 6 scans per series have been chosen in order to cover the cross-section largely. A schematic illustration of this procedure is shown in Fig. 5.

At first two series with the reduced beam height were executed. Afterwards the slit aperture has been removed and another scan with the full beam cross-section, i.e. exposing the entire cell to the beam again, has been done. Finally, the slit aperture has been mounted again and one further series has been taken. In total, four scans three of which with the slit aperture and one without have been executed.

The first series from anode to cathode was done during startup at no load. No influence on the cell voltage was observed and the OCV prior to putting the cell under load was 925 mV. After the first series the cell was put under load with 0.14 A cm^{-2} constant current density, and a second series was started. The first and second scan of this series were done at the anode and did not indicate a strong correlation between beam exposure and voltage. Moving the beam further to the cathode side of the cell, scans 3–6 cause clearly visible voltage responses to beam exposure. These observations indicate that predominantly the cathode materials interact with the beam whereas the anode materials seem to be less sensitive.

Fig. 6 shows an exemplary and representative result for the observations made during the series under load as described above. The figure depicts the cell behavior during the third series (full beam exposure under load). The cell was operated with a constant current density of 0.14 A cm^{-2}. Despite of the fact that some detrimental interaction of the SR beam with the materials in the cell during the two preceding series has to be assumed the cell is leveling out at approx. 320 mV before being exposed to the beam again. With the cell being largely stable at 320 mV, one full scan was executed. The cell voltage decayed completely, and after reaching zero potential the electronic load was not able to maintain the current. After switching-off the load, though, a reasonable OCV of 930 mV was obtained. However, it was impossible to get the cell in operation again afterwards. The voltage loss was irreversible despite of the normal OCV.

After the fully exposed scan (Fig. 6), the slit aperture has been mounted again for the final series. Since the cell could not be recovered to draw current, though, just OCV could be studied regarding beam exposition. As shown in Fig. 7, scans with the anode exposed to the beam (i.e. scans 1–3) seem to keep the OCV unaffected. In contrast to that, scans that expose the cathode to the beam (scans 4–6) result in a drop of the OCV which stabilizes at a lower level and seems to be reversible after the beam is switched off. This finding seems to contradict to what has been found during the scan at startup, and it has to be concluded that there is a beam/cell interaction even under OCV if the cell had been operated under beam exposure before.

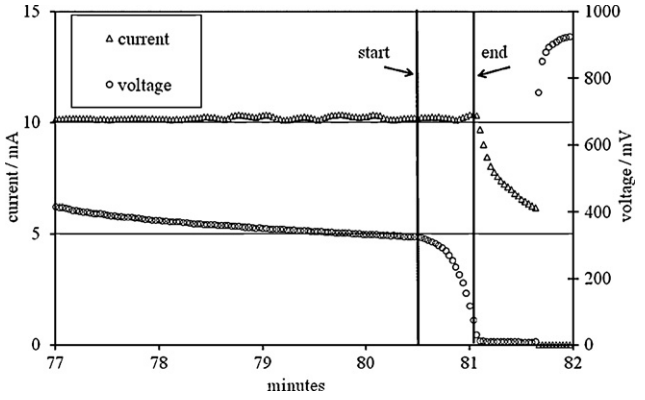

Fig. 6. The fuel cell operation at nearly constant conditions before and after applying synchrotron radiation. During the beam exposure for one tomography the cell voltage crashed and no further operation was possible.

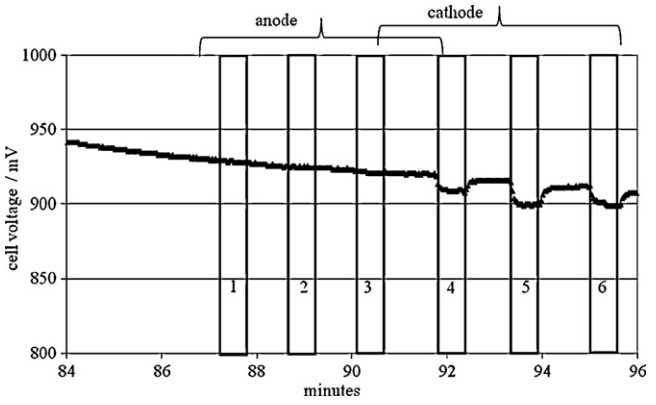

Fig. 7. A series of 6 scans in different areas of the fuel cell at OCV was recorded. The first scan starts in the region of the anode diffusion media and the last ends in the region of the cathode diffusion media.

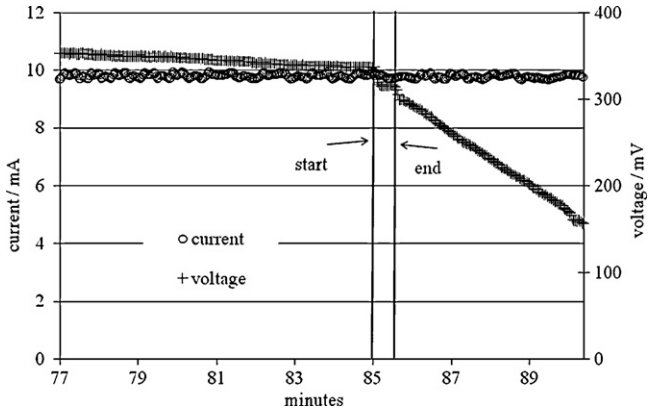

Fig. 8. The fuel cell operation during synchrotron radiation. Marked are the positions when the beam exposure starts and ends.

The above observations have been confirmed in several cell builds. As an example, Fig. 8 shows another cell build with the entire cell exposed to the beam. The fuel cell was operated at 0.14 A cm^{-2} for about 10 min and behaved normally until a full scan over the whole setup was applied. The start and the end of this scan are marked in the figure. Although the beam exposure was only 30 s the voltage decreased after the scan much faster than before. This could indicate irreversible changes of material properties.

3.3. Imaging

Despite of the above findings that may question the applicability of SR at this point in time, imaging data sets have been acquired. The images are obtained by phase-contrast imaging in the so-called edge detection regime [8], and the 3D data set has been reconstructed afterwards. As an example, a reconstructed data set is shown in Fig. 9. The reconstructed area is about 2.8 mm in diameter and shows clearly the flow field geometry with the adjacent carbon fiber structure of the gas diffusion layer.

As an example, Fig. 10 shows a perspective view into a full 3D imaging data set obtained during fuel cell operation. The catalyst layers on both sides of the membrane are clearly visible in the cross-sectional cut. For illustrative reasons, the cathode is displayed on the top side and the anode on the bottom side. In the diffusion media bright areas correspond to the carbon fibers whereas dark areas represent the free gas space, i.e. gas-filled pores. The medium grey-scale values represent areas filled with water. Consistent with the expectation much more water has been found on the cathode side.

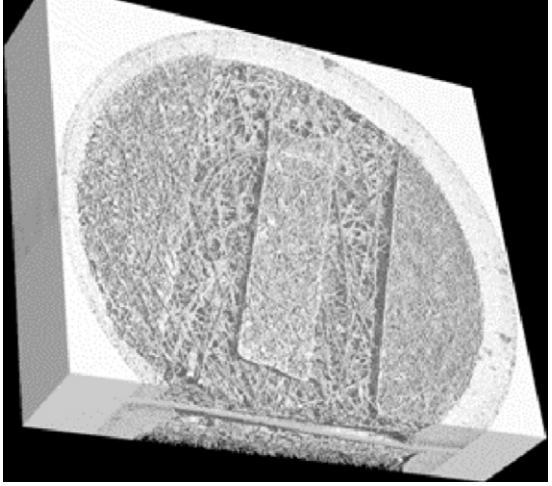

Fig. 9. Reconstructed 3D imaging data set of the micro fuel cell. The two channel structure of one flow field and a gas diffusion media are visible.

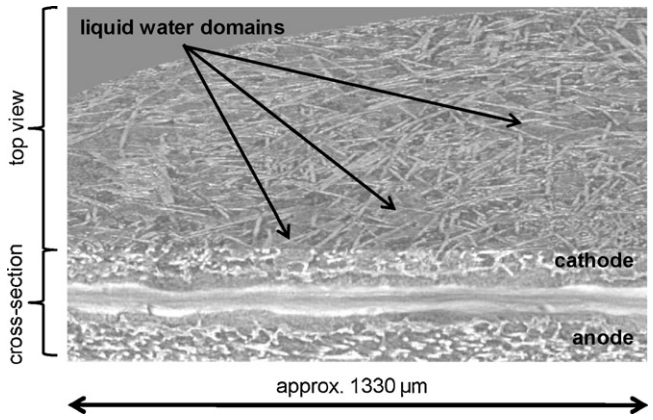

Fig. 10. Representative imaging data set obtained during fuel cell operation showing liquid water filling part of the pore space between the fibers of the diffusion medium (perspective view).

Qualitatively, the degree of liquid saturation seems to be high. In order to quantify the saturation and clarify the water transport mechanisms, though, accurate image processing of the data is required. The major challenge in that regard is namely the segmentation, of the gray-scale data sets to clearly identify solid, liquid and pore volumes. The spatial resolution of 2.8 μm (voxel size) chosen here clearly complicates the segmentation process as the edges between the phases (solid, void and liquid) seem to be foggy. As shown by Flückiger et al. [3] such an analysis might be facilitated by increasing spatial resolution down to 1 μm or even less. However, it has to be clarified whether the trade-off with temporal resolution remains reasonable if such high spatial resolution is used.

4. Discussion

As described above and illustrated in Fig. 6 the decay of the fuel cell performance takes place with rates that are in the same order of magnitude as the transients of the water transport mechanisms that are the actual objective of the imaging experiment. Manke et al. [4], for instance, indicate time constants of approx. 1 min for the periodic water transport while the performance degradation observed here was in the order of 30 s for complete voltage decay.

First of all, it has to be speculated whether the design specifics of the micro fuel cell, the challenging cell assembly or the dry operating conditions cause performance degradation that is not representative for a technical fuel cell. However, the comprehensive cell qualification in the absence of any beam exposure demonstrated stable cell operation. Furthermore, the large amount of water visible in the imaging data (Fig. 10) suggests that despite of using dry inlet gases humid or even wet conditions exist in the porous gas diffusion medium. Hence, attributing the fading performance to the dry conditions does not hold, as reflected by the stable operation in the absence of the beam. Besides that, the qualitatively high liquid saturation emphasizes the need to hydrophobically treat the diffusion medium in order not to get flooded with liquid water and maintain the wetting properties of the surface. For that reason it would be of particular concern if the performance loss was caused by a beam-induced material degradation of the hydrophobic PTFE treatment. In that regard, the scanning experiment indicated strongly a higher beam sensitivity of the cathode where the product water is generated. This might give a hint to a correlation of performance degradation with deteriorated water

management caused by increasing wetting of the solid surfaces. In fact, interaction of water and X-rays resulting in a decrease of the natural surface tension of water has been observed [12]. Even in the absence of any PTFE degradation a lower surface tension of the product water would necessarily increase the wetting and, hence, the liquid saturation of the pore space with liquid product water. However, material degradation through X-ray irradiation in terms of changing composition actually has been observed. Himmerlich et al. [13] studied the changes of PTFE-like fluorocarbon films exposed to soft X-ray radiation and observed a strong decrease of the fluorine-to-carbon ratio of the fluorocarbon surfaces. This defluorination strongly reflects the decomposition of the surface. As wetting is a surface rather than a bulk mechanism, even small modifications of the surface composition may lead to severe changes of the wetting properties. Kanda et al. [14] exposed PTFE to synchrotron radiation and measured the wetting behavior afterwards. They found that at room temperature the contact angle of water on PTFE decreased severely with increasing SR dose. However, the doses applied by them were in the order of tens and hundreds of mA h. In our case, with ring currents of approx. 200 mA and fuel cell decay in less than 1 min, doses were rather in the order of 1 mA h. Nevertheless, even in case of small separate impact of the individual mechanisms, i.e. reduced surface tension and PTFE degradation, both mechanisms may aggravate and lead to the observed high performance degradation rates. Besides PTFE, interaction of X-rays and SR beams with PFSA-based polymer electrolyte membranes has been reported [15]. From the perspective of fuel cell operation, a loss of sulfuric acid groups, for instance, would be directly reflected in a performance loss due to lower membrane ion conductivity. This should not affect, though, the OCV which has been observed here. However, degradation products of membrane decomposition during beam exposure may poison the Pt catalyst. For instance, sulfur and sulfur compounds are known as strong catalyst poisons [16,17]. Since the active groups in PFSA membranes are sulfuric acid, any loss of these is a potential source for catalyst poisoning. A particular irradiation sensitivity of the side-chains that attach the acid groups to the polymer backbone of the membrane has been reported previously [18]. Besides that, the backbone of PFSA membranes is PTFE which is, as mentioned above, prone to beam-induced decomposition. Apart of CO_2 as a decomposition product of PTFE, CO is produced, too [19]. Like sulfur compounds, CO is a strong catalyst poison and will immediately deteriorate cell performance. The high excess of O_2 in the cathode gas, though, should oxidize CO from the catalyst surface and, hence, restore performance after poisoning fast. This effect is utilized to mitigate CO contamination in hydrogen-rich reformate fuels by adding small amounts of air to the anode feed [17]. However, the low sensitivity of the anode to beam exposure observed here may rule out CO as a contaminant.

The potential mechanisms due to beam/material interaction leading to performance degradation may be summarized as follows:

- decrease of water surface tension and PTFE decomposition causing increased wetting of pore space and potential flooding,
- decomposition of PFSA-based polymer electrolyte membrane reducing membrane conductivity (loss of sulfuric acid groups),
- decomposition of PTFE and PFSA membrane causing catalyst poisoning by decomposition products (CO, S),
- a combination of these mechanisms.

However, based on discussed literature the potential mechanisms should occur at low radiation energies only. For instance, binding energy of C–C and C–F bonds are 284 and 697 eV, respectively [14]. Publications reporting fluoropolymer degradation therefore utilized soft X-rays or low-energy synchrotron radiation. Hence, dissociation of these bonds is not to be expected for the SR application reported here where beam energies of >20 keV have been used. If so far not understood mechanisms exist that either lead to the discussed mechanisms or which generate low-energy fractions in the beam is currently being studied. The general degradation of the MEA caused by the mere fuel cell operation itself is subject of numerous publications that also aim at identifying the individual anode and cathode sensitivities [20,21]. It has to be noted, though, that typical in situ lifetime tests like those referenced here are in the order of hundreds and thousands of operating hours in order to observe significant performance degradation. This is in sharp contrast to our observation where severe performance degradation under beam exposure is in the order of tens of seconds. Hence, beam-induced degradation cannot be understood as being relevant to actual fuel cell operation. Whether beam exposure acts as an accelerating factor for degradation mechanisms that may occur in regular fuel cell operation but on a very different time scale needs to be further investigated. Unfortunately, the amount of sample from an in situ SR experiment with full exposure of the entire active area is not sufficient for typical analytical material characterization methods.

The above findings seem to contradict other results obtained on operating fuel cells imaged with SR. Despite of electrochemical operation during exposure, no performance degradation has been reported. This circumstance should be due to the fact, as indicated in the introduction, that different from our experiment either not the entire active area has been exposed to the beam or the electrochemical behavior of the cell has not been actively controlled or monitored. For instance, experiments reported by [4,6,7] exposed only a fraction of the cells to the beam while unintentionally shielding the active area largely from the beam. Hereby any degradation of the exposed area will not be visible in the overall current–voltage behavior which is dominated by the unexposed active area. It has to be concluded that only a fully exposed active area provides the sensitivity of the electrical signal to reveal the degradation effect. On the other hand, experiments which operate electrochemically to generate product water but do not monitor the electrical signals, e.g. [3] simply do not detect the performance degradation.

A worst case implication of these observations could be the non-applicability of SR imaging to fuel cells due to severe degradation of fuel cell materials under beam exposure. Hence, any conclusion drawn from such imaging might be misleading as the materials are not longer representative for undegraded fuel cell materials. For example, if it is the hydrophobic treatment that degrades, any interpretations relating to the distribution and movement of liquid water in the GDL might not be applicable to actual fuel cells. These questions are currently under investigation.

5. Conclusions

For the purpose of SR imaging of the entire active area a miniaturized fuel cell and peripheral equipment for controlled fuel cell operation during the imaging have been developed. The micro cell has been well characterized and representative performance has been demonstrated. Operation at the imaging facility showed a significant correlation between SR beam exposure and fuel cell performance. Under OCV the impact of irradiation seems to depend on the history of the fuel cell operation and indicated that the OCV can be regenerated if the beam is switched off. Under load, however, cell performance decreases seriously and with fast rates indicating that the beam induces high degradation rates on fuel cell materials. This seems to contradict other published in situ SR imaging results. However, so far no imaging experiment that operates a fuel cell with controlled voltage and current and exposes the entire active area to the beam has been demonstrated yet. This is assumed to be the key aspect for making the degradation observation reported

here. First results did not indicate that these effects are reversible since the cell that had been tested could not be recovered. Preliminary tests suggest that the cathode is more sensitive to beam exposure compared to the anode. Based on the observations and literature data on material/beam interaction it can be speculated that key properties of typical fuel cell materials, e.g. wetting properties of the PTFE-based hydrophobic treatment or ion conductivity of the polymer electrolyte membrane, may change under exposure. Besides this, poisoning of the Pt catalyst with decomposition products may occur. However, it is unclear yet if the observations published here in the end actually relate to a degradation of the porous, hydrophobically treated diffusion medium. Since the water transport in the diffusion medium is the subject of the SR imaging investigation any beam-induced material degradation that changes its wetting properties introduces non-negligible artifacts. Consequently, before further in situ imaging studies are going to be executed, a clarification of the interaction of synchrotron radiation and fuel cell materials is required. This clarification is subject of currently ongoing investigations. If such an interaction with high degradation rates in the order of minutes or even faster can be confirmed, interpretations of SR imaging results with regard to water transport mechanisms in the actual fuel cell application have to be made carefully.

Acknowledgements

The authors would like to thank the European Synchrotron Radiation Facility for providing the beam time, Pascal Bernard and Jean-Paul Valade for mechanical design and installation, Paul Nicotera and Abel Chuang for discussing experimental details, Steffen Böhm for supporting cell design and especially Wolfgang Herud for an excellent support regarding the test periphery.

References

[1] J. St-Pierre, J. Electrochem. Soc. 154 (2007) B724–B731.
[2] A. Bazylak, Int. J. Hydrogen Energy 34 (2009) 3845–3857.
[3] R. Flückiger, D. Tehlar, F. Marone, M. Stampanoni, A. Wokaun, F.N. Büchi, Determination of liquid water distribution in PEFC by X-ray tomography, Annual Report Electrochemistry Laboratory, Paul-Scherrer Institute Switzerland, 2008.
[4] I. Manke, Ch. Hartnig, M. Gruenerbel, W. Lehnert, N. Kardjilov, A. Haibel, A. Hilger, J. Banhart, H. Riesemeier, Appl. Phys. Lett. 90 (2007) 174105.
[5] Ch. Hartnig, I. Manke, R. Kuhn, N. Kardjilov, J. Banhart, W. Lehnert, Appl. Phys. Lett. 92 (2008) 134106.
[6] Ch. Hartnig, I. Manke, R. Kuhn, S. Kleinau, J. Goebbels, J. Banhart, J. Power Sources 188 (2009) 468–474.
[7] T. Mukaide, S. Mogi, J. Yamamoto, A. Morita, S. Koji, K. Takada, K. Uesugi, K. Kajiwara, T. Noma, J. Synchrotron Radiat. 15 (2008) 329–334.
[8] P. Cloetens, M. Pateyron-Salomé, J.Y. Buffière, G. Peix, J. Baruchel, F. Peyrin, M. Schlenker, J. Appl. Phys. 81 (1997) 5878.
[9] P. Cloetens, W. Ludwig, E. Boller, L. Helfen, L. Salvo, R. Mache, M. Schlenker, Quantitative phase contrast tomography using coherent synchrotron radiation, in: U. Bonse (Ed.), Proceedings SPIE: Developments in X-ray Tomography III, vol. 4503, 2002, 8291 pp.
[10] T. Martin, A. Koch, J. Synchrotron Radiat. 13 (2006) 180–194.
[11] URL http://www.esrf.fr/UsersAndScience/Experiments/TBS/SciSoft/.
[12] B.M. Weon, J.H. Je, Y. Hwu, G. Margaritondo, Phys. Rev. Lett. 100 (2008) 217403.
[13] M. Himmerlich, V. Yanev, A. Opitz, A. Keppler, J.A. Schaefer, S. Krischok, Polym. Degrad. Stabil. 93 (2008) 700–706.
[14] K. Kanda, T. Ideta, Y. Haruyama, H. Ishigaki, S. Matsui, Jpn. J. Appl. Phys. 42 (2003) 3983–3985.
[15] M. Pineri, G. Gebel, R. Davies, O. Diat, J. Power Sources 172 (2007) 587–596.
[16] D. Imamura, Y. Hashimasa, ECS Trans. 11 (1) (2007) 853–862.
[17] X. Cheng, Z. Shi, N. Glass, L. Zhang, J. Zhang, J. Power Sources 165 (2007) 739–756.
[18] M. Schulze, M. Lorenz, N. Wagner, E. Gülzow, Fresenius J. Anal. Chem. 365 (1999) 106–113.
[19] M. Schulze, A. Schneider, E. Gülzow, J. Power Sources 127 (2004) 213–221.
[20] L. Ghassemzadeh, M. Marrony, R. Barrera, K.D. Kreuer, J. Maier, K. Müller, J. Power Sources 186 (2009) 334–338.
[21] M. Holber, A. Carlsson, P. Johansson, L. Jörissen, P. Jacobsson, ECS Trans. 25 (1) (2009) 807–811.